Editors' Suggestion

Optically trapped microspheres are high-bandwidth acoustic transducers

L.E. Hillberry and M.G. Raizen*
Department of Physics, The University of Texas at Austin, Austin, Texas 78712, USA

(Received 29 September 2023; revised 4 December 2023; accepted 15 December 2023; published 18 January 2024)

We report on the use of an optically trapped microsphere as an acoustic transducer. A model for the hydrodynamic coupling between the microsphere and the surrounding acoustic fluid flow is combined with thermomechanical calibration of microsphere-position tracking to enable quantitative acoustic measurements. We describe our technique in detail, including the self-noise, the sensitivity, and the minimum detectable signals, using a model appropriate for both liquid and gas environments. We then test our approach in an air-based experiment and compare our measurements with two state-of-the-art commercially available acoustic sensors. Piezoelectrically driven bursts of pure tones and laser ablation provide two classes of test sounds. We find that accurate measurements with a bandwidth of 1 MHz are possible using our technique, improving by several orders of magnitude the bandwidth of previous flow measurements based on optically trapped microspheres.

DOI: 10.1103/PhysRevApplied.21.014031

I. INTRODUCTION

Owing to their micromanipulation and force-transduction capabilities, optical tweezers have become an indispensable tool in a variety of scientific fields [1]. By tightly focusing a laser beam, optical forces can exceed gravitational forces and thermal fluctuations to stably trap micron-scale objects [2]. In vacuum [3], optical tweezers have enabled zeptonewton force sensing [4], state-of-the-art torque sensitivity [5], and searches for new physics [6], including proposals to measure high-frequency gravity waves [7]. Also in vacuum, optical tweezers can trap and cool microspheres [8] to the motional ground state [9,10] and have been multiplexed to arrays of hundreds of single-atom traps in a promising platform for quantum computation and simulation [11,12]. In aqueous solution, optical tweezers can measure mechanical properties of life at the nanoscale [13,14], such as the stepping strength of molecular motors or the rigidity of biomolecules [15–17]. Also in liquid, optical tweezers enable ultrafast viscosity measurements [18] and Casimir force measurements [19]. In gaseous media, optical tweezers have revolutionized single-particle aerosol science [20], including absolute pressure measurements and species identification [21], mass metrology [22,23], and single-droplet growth and freezing studies [24–26].

There further exists a body of work using optically trapped microspheres to measure flow in liquids [27–32]. So far, these studies have characterized low-frequency (< 500 Hz) flows by monitoring the motion of optically trapped microspheres with a camera or position-sensitive detector. In this paper, we propose and demonstrate a fluid-velocity measurement scheme with a bandwidth approaching 1 MHz using optically trapped microspheres in air. Flow at such high frequencies is generally associated with acoustic radiation. A schematic of our optically trapped microsphere acoustic transducer is shown in Fig. 1. Other nontraditional acoustic sensors have recently been studied, including optical microresonators [33,34] and laser deflection or interference methods [35]. As we will see, our method combines self-calibration, high bandwidth, and high sensitivity to acoustic velocity waves (rather than pressure waves).

Our method builds on earlier work that resolved the instantaneous velocity of a thermally fluctuating microsphere in air [36]. High-spatiotemporal-resolution position tracking along one dimension is achieved by monitoring the optical interference between unscattered and forward-scattered trapping light [36,37] (see Fig. 1 for a schematic and [38] for a recent analysis). This same system is not only sensitive to thermal fluctuations but also to acoustic perturbations. Two ingredients, a hydrodynamic model of the acoustic force and thermomechanical self-calibration, enable quantitative acoustic measurements. Since the microsphere is uniquely sensitive to high-frequency velocity flows, we use two commercially available sensors to assess the capabilities of our platform. We benchmark our method in terms of accuracy and bandwidth against (1) a high-bandwidth (200 kHz) pressure microphone, and (2) a micron-scale dual-hot-wire anemometer [39,40] (calibrated bandwidth 20 kHz) that is commercially known as the *Microflown* [41].

*lhillber@utexas.edu

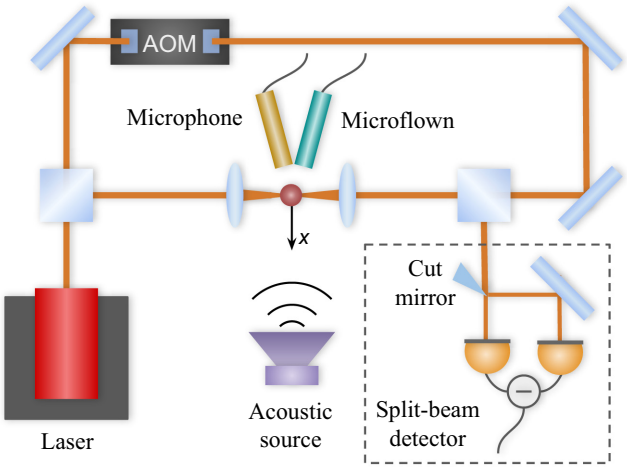

FIG. 1. A schematic depiction of the experimental setup. A 1064-nm laser is split by a polarizing beam splitter. The p-polarized beam is sent through an acousto-optic modulator (AOM) to shift its frequency by 80 MHz, thereby eliminating interference effects in the trap. The p-polarized beam is then steered counterpropagating to the s-polarized beam and both are focused to the same point between twin aspheric lenses (numerical aperture 0.7), generating a stable optical trap for silica microspheres in air. After passing through the trap, the s-polarized beam is separated with a second polarizing beam splitter and sent to the detection system. For detection along the x direction, a sharp, D-shaped mirror splits the transverse mode into two halves that are sent to a balanced photodetector (75 MHz bandwidth). Various acoustic sources provide test sounds and additional acoustic sensors, a microphone and the Microflown, are positioned just behind the trap. The entire system is enclosed in a multichamber acrylic box to mitigate air currents.

The remainder of this paper is organized as follows. In Sec. II, we describe the acoustic sensing modality of the microsphere, including calibration, self-noise, and minimum detectable signals. Section III reports our sound-detection results. We then discuss our results within the context of other microsphere-based flow measurements and speculate on future applications in Sec. IV. The paper is then concluded in Sec. V.

II. NOISE, CALIBRATION, AND ACOUSTIC RESPONSE

In thermal equilibrium with a reservoir fluid at finite temperature, the position of a microsphere fluctuates in random and perpetual *Brownian motion* [42]. Brownian-motion velocity detectors [18,36,43] are sensitive to both thermally fluctuating and driven fluid flows. If the resulting driven motion is larger than the random thermal motion (and detector noise), an acoustic signal is detectable. In what follows, we develop a model for the acoustic signal and thermal noise of our proposed acoustic detection system.

For the general setup, consider a microsphere of radius R and density ρ harmonically bound to the coordinate origin. The microsphere mass is $m = 4\pi\rho R^3/3$ and the harmonic trap strength is κ. Let the trapping fluid at temperature T have density ρ_f, speed of sound c_0, and dynamic viscosity η. The x component of the equation of motion of the system is

$$m\ddot{x}(t) + \kappa x(t) - F_\mathrm{d}[v(t)] = F_\mathrm{ext}(t) + F_\mathrm{th}(t), \qquad (1)$$

where $v(t) = \dot{x}(t)$ is the velocity of the microsphere at time t, $F_\mathrm{d}(v)$ is the dissipative velocity-dependent drag force, and F_ext is an external driving force. F_th is the fluctuating thermal force, which is related to the dissipative force through the fluctuation-dissipation theorem.

When all bounding walls are far from the sphere [44] and the fluid flow at the surface of the sphere does not slip [45], the hydrodynamic drag force in the incompressible limit is [46–48]

$$F_\mathrm{d}[v(t)] = -\gamma_0\left(v(t) + \sqrt{\frac{\tau_\mathrm{f}}{\pi}}\int_{-\infty}^{t} \mathrm{d}t' \, \frac{\dot{v}(t')}{\sqrt{t-t'}}\right) - \frac{\delta}{2}m\dot{v}(t), \qquad (2)$$

where $\gamma_0 = 6\pi\eta R$ is the Stokes friction coefficient and $\delta = \rho_\mathrm{f}/\rho$ is the fluid-to-microsphere density ratio. The *vorticity diffusion time* $\tau_\mathrm{f} = R^2\rho_\mathrm{f}/\eta = 9\delta\tau_\mathrm{p}/2$ is the amount of time it takes for the vorticity—the curl of velocity—to diffuse across the sphere and $\tau_\mathrm{p} = m/\gamma_0$ is the momentum diffusion time. The first, second, and third terms of Eq. (2) describe, respectively, the Stokes drag (independent of δ), the viscous damping due to the flow history (proportional to $\delta^{1/2}$), and the inertia of the mass added by the fluid that follows the microsphere (proportional to δ). For a silica microsphere in air, $\delta \sim 10^{-3} \ll 1$; hence Eq. (2) reduces to $F_\mathrm{d}[v(t)] \approx -\gamma_0 v(t)$.

In the frequency domain, we may write $F_\mathrm{d}[v(\omega))] = -\gamma(\omega)v(\omega)$, where $\omega = 2\pi f$ is the circular frequency, the frequency-dependent damping is [49,50]

$$\gamma(\omega) = \gamma_0\left(1 + \sqrt{-i\tau_\mathrm{f}\omega} - i\frac{\tau_\mathrm{f}\omega}{9}\right), \qquad (3)$$

and $\sqrt{-i} = (1-i)/\sqrt{2}$ defines the branch cut of the square root.

Next, we consider two cases: *noise* when $F_\mathrm{ext} = 0$ and *signal* when $F_\mathrm{th} = 0$ and F_ext is caused by an acoustic wave.

A. Noise

The thermal force is $F_\mathrm{th}(t) = \sqrt{2k_\mathrm{B}T\gamma_0}\xi(t)$, where $\xi(t)$ is a zero-mean possibly time-correlated [53] random variable and k_B is Boltzmann's constant. When $F_\mathrm{ext} = 0$, the equation of motion given in Eq. (1) may be solved in the frequency domain for the *admittance* $v(\omega)/F_\mathrm{th}(\omega) =$

$(\gamma(\omega) - i\omega m + i\kappa/\omega)^{-1}$ The corresponding (one-sided) velocity power spectral density is given by the Kubo-Green formula [54] as

$$S_{vv}(\omega) = 4k_B T \,\mathrm{Re}\left[(\gamma(\omega) - i\omega m + i\kappa/\omega)^{-1}\right]. \quad (4)$$

Equation (4) describes the thermal fluctuations of the microsphere and hence the inherent noise that must be overcome to detect $F_{\mathrm{ext}} \neq 0$. However, beyond noise limitations, thermal fluctuations enable an accurate detector-calibration scheme.

The split-beam-detection method, depicted in Fig. 1, generates a linear voltage signal $V(t) = \beta x(t)$, where β is the displacement-to-voltage calibration factor. For silica microspheres in air, the radius R, temperature T, and viscosity η can be considered known to within a couple of percent [22,51,55]. Since $S_{xx} = S_{vv}/\omega^2$, we can predict the (one-sided) Brownian-motion-driven voltage power spectral density of the detector

$$S_{VV}(\omega) = \frac{\beta^2}{\omega^2} S_{vv}(\omega) \quad (5)$$

$$\approx \beta^2 \frac{4k_B T \gamma_0}{(m\omega^2 - \kappa)^2 + \gamma_0^2 \omega^2}. \quad (6)$$

The second approximate equality, given in Eq. (6), is accurate for thermal fluctuations in air and assumes $\gamma(\omega) \approx \gamma_0$. As shown in Fig. 2(a), by averaging experimental periodograms of thermally driven voltage signals and maximum-likelihood fitting [52,56] to Eq. (6), we can learn [22] $\rho = 1.7(1)$ g/cm^3, $\kappa = 21.3(7)$ fN/nm, and $\beta = 2.1(1)$ mV/ nm. At high frequencies, the spectrum given in Eq. (6) decays as ω^{-4} until the constant noise floor $\chi = 0.49(2)$ mV^2/Hz of the detector dominates the signal. The narrow-band position sensitivity of our detector is therefore $\sqrt{\chi}/\beta = 333(21)$ fm/$\sqrt{\mathrm{Hz}}$. The inset of Fig. 2(a) shows that subtle hydrodynamic effects described by Eq. (5) are perceptible in thermally driven motion above approximately 50 kHz but may be ignored for calibration purposes by restricting the fit domain. In Sec. II B, we will calculate the response of the microsphere to a harmonic acoustic wave.

B. Signal

When impinging on the trapped microsphere along the x direction of position measurement, a sound wave of fluid velocity u and acoustic pressure p applies an external force [48] $F_{\mathrm{ext}} = F_\nabla(p) + F_{\mathrm{d}}(-u)$. The pressure-gradient force is $F_\nabla(p) = -4\pi R^3 \nabla p/3$. Using Euler's (linearized) equation $\nabla p = -\rho_{\mathrm{f}} \dot{\mathbf{u}}$, the pressure-gradient force is $F_\nabla = \delta m \dot{u} = 2\gamma_0 \tau_{\mathrm{f}} \dot{u}/9$. Taking $F_{\mathrm{th}} = 0$, one can solve the equation of motion given in Eq. (1) in the frequency domain for the transfer function $H(\omega) = v(\omega)/u(\omega)$, yielding

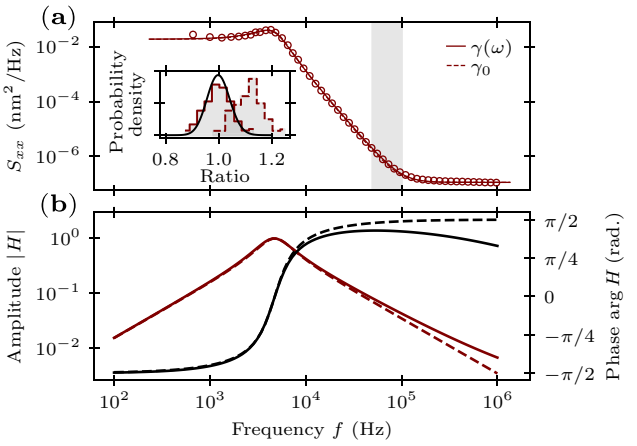

FIG. 2. (a) The experimental position power spectral density (open circles) of a $R = 1.51(5)$ μm silica microsphere thermally driven by air at $T = 23.97(1)^\circ$C with a relative humidity of 57(1)%, which has a viscosity of $\eta = 18.23(1)$ μPa s [51]. The experimental spectrum is an average periodogram of 550 signals of length 3 ms. For visualization, each point of the experimental spectrum is an average over logarithmically spaced frequency bins. Calibration is performed by fitting the voltage spectrum in the 1–30 kHz band to Eq. (6) (dashed line). The spectrum and fit are shown here in physical units using the calibration result. The solid line uses the fit results to include hydrodynamic effects that are imperceptible up to approximately 50 kHz. However, the 50–100 kHz band (gray shaded region) does exhibit subtle hydrodynamic effects, as suggested by the probability density of the data-to-theory ratio (inset), wherein the hydrodynamic theory (solid red line) follows much more closely the expected Erlang distribution of ratios (solid black line) [22,52]. (b) The theoretical transfer function relating microsphere velocities to fluid velocities. The red lines show the amplitude on the left axis, while the black lines show the phase on the right axis. The solid line corresponds to the hydrodynamic theory, while the dashed lines makes the approximation $\gamma(\omega) \approx \gamma_0$. The microsphere, trap, and fluid parameters are chosen to be consistent with the calibration shown in (a).

$$H(\omega) = \frac{\gamma(\omega) - i\omega\delta m}{\gamma(\omega) - i\omega m + i\kappa/\omega}. \quad (7)$$

The transfer function, shown in Fig. 2(b), describes the velocity amplitude and phase of the microsphere relative to that of the fluid. Although $\gamma(\omega) \approx \gamma_0$ is appropriate for thermal fluctuations and system calibration in air, driven motion can occur at much higher frequencies, so we retain all three terms in Eq. (3). For example, at 1 MHz, taking $\gamma(\omega) \approx \gamma_0$ underestimates the amplitude of H by a factor of approximately 2 and overestimates the phase by approximately $\pi/6$ radians. The primary correction to H beyond $\gamma(\omega) \approx \gamma_0$ comes from the history term in Eq. (3); the added mass and pressure-gradient effects are both proportional to the density ratio δ and hence are small in air. We

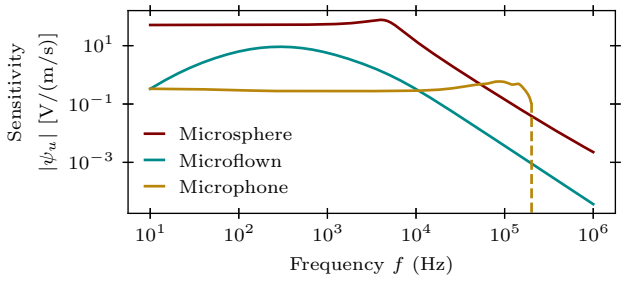

FIG. 3. Comparing acoustic detector velocity sensitivities. The microsphere parameters are consistent with the calibration shown in Fig. 2(a). The microphone sensitivity is provided by the manufacturer and includes corrections for operation without the protective grid and in free-field conditions. The nominal pressure sensitivity is 0.68 mV/Pa and is converted to velocity via the plane-wave impedance of air for comparison with the velocity sensors. The microphone calibration is known up to 200 kHz (dashed amber line).

retain all terms so that our model remains valid for liquid media for which $\delta \sim 0.1-1$.

The voltage signal of the detector is converted to an acoustic velocity signal using a frequency-domain deconvolution $u(t) = \mathcal{F}^{-1}[\mathcal{F}[V(t)]/\psi_u(\omega)]$, where $\mathcal{F}$ is the Fourier transform, and the frequency-dependent velocity sensitivity of the microsphere is

$$\psi_u(\omega) = \frac{-i\beta H(\omega)}{\omega}. \tag{8}$$

The sensitivity is proportional to the transfer function H, the calibration factor β, and the factor $-i/\omega$ that affects the required position-to-velocity derivative. For experimental data sampled at a rate $1/dt$, the derivative factor consistent with a central finite difference in the time domain is $-i/\omega \to -idt/\sin(\omega dt)$ [57]. The acoustic pressure and velocity are related through the impedance $Z(\omega) = p(\omega)/u(\omega)$; hence the pressure sensitivity is $\psi_p = \psi_u/Z$. For plane acoustic waves, $Z = \rho_f c_0$ is a constant. We will assume planar acoustic waves throughout and use the factor Z to freely convert between pressure and velocity.

Commercial acoustic detectors are typically calibrated by comparing the output voltage of the sensor to a well-characterized input sound under anechoic conditions. By contrast, our thermomechanical position calibration and hydrodynamic transfer function enable self-calibration. The sensitivity amplitudes of our commercial microphone and the Microflown are provided by the manufacturers and are shown in Fig. 3 compared to the sensitivity of our microsphere system. All measurements reported herein are converted to physical units using the appropriate sensitivity curves.

C. Detection limits

The above considerations for signal and noise allow us to estimate the minimum detectable acoustic signal of our microsphere. A voltage signal derived from only thermal fluctuations given in Eq. (5) and then transformed to a fluid velocity via the sensitivity given in Eq. (8) will exhibit a self-noise spectrum [Fig. 4(a)]

$$S_{\mathrm{nn},u}(\omega) = \frac{S_{VV}(\omega)}{|\psi_u(\omega)|^2} = \frac{4k_B T \mathrm{Re}[\gamma(\omega)]}{|\gamma(\omega) - i\omega\delta m|^2}. \tag{9}$$

The self-noise is quite flat and near the dc value $S_{\mathrm{nn},u}(\omega \to 0) = 4k_B T/\gamma_0$. From the self-noise spectrum, the minimum detectable signal is given by the band-limited variance [Fig. 4(b)] $u_{\min} = \sqrt{\int_0^f \mathrm{d}f' S_{\mathrm{nn},u}(2\pi f')}$. One can include the effects of a constant detector-noise floor by making the replacement $S_{VV}(\omega) \to S_{VV}(\omega) + \chi$ in Eq. (9). In addition to predicting the self-noise of our microsphere system, Fig. 4 reports the measured self-noise of all of our sensors, found by analyzing signals in the absence of acoustic drive. However, our self-noise measurements are not performed in an anechoic chamber and therefore include significant environmental noise extrinsic to any device limitations.

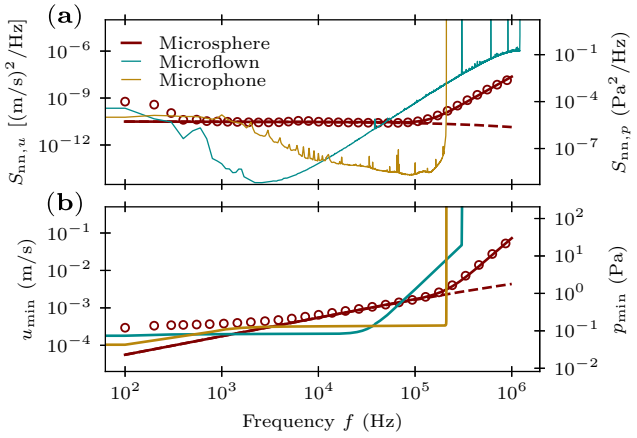

FIG. 4. (a) The self-noise spectra for each acoustic sensor. The Microflown and microphone curves correspond to experimental measurements and therefore include environmental noise (concentrated below 1 kHz) as well as self-noise contributions. Similarly, the red data points correspond to microsphere self-noise measurements but averaged over logarithmically spaced frequency bins for visual clarity. (b) The minimum detectable acoustic disturbances estimated from the self-noise spectra band-limited variances. High-frequency electronic resonances in the Microflown spectrum and a sharp bandwidth cutoff in the microphone spectrum induce diverging minimum detectable acoustic amplitudes. In both panels, the solid red lines correspond to the model given in Eq. (9), including effects of a constant detection-noise floor, while the dashed line assumes perfect detection.

III. RESULTS

Having established the operating principle and expected performance of optically trapped microspheres as acoustic sensors, we next describe the experimental results. Using a two-channel high-speed digitizer, we record the microsphere signal and either the microphone or the Microflown signal when driven by various sound sources. Each channel is analog-low-pass filtered to 4 MHz and then sampled at a rate of $1/dt = 25$ MHz to minimize aliasing. In postprocessing, the recorded voltage signals are further low-pass filtered by averaging together adjacent points of nonoverlapping segments, thereby adjusting the effective sampling rate and signal bandwidth. Once filtered, the voltage signals are converted to either pressure or velocity using the appropriate sensitivity curves.

A. Tone-burst sound source

Tone bursts, consisting of a certain number of sinusoidal cycles at a single frequency, provide a simple and repeatable test signal for our various acoustic detectors. In our first set of experiments, we launch tone busts using a function generator to drive piezoelectric buzzers held a distance $\Delta x = 44$ mm from the optical trap. Δx is varied by mounting the piezo buzzers on a motorized platform. We drive one of two buzzers at their resonant frequencies 4 kHz or 40 kHz. We observe excellent agreement between our commercially calibrated reference sensors and our thermomechanically calibrated research system, as shown in Fig. 5. The agreement between sensors lessens as the source distance Δx or time t increases (see Fig. 7 of the Appendix). The loss of agreement could be due to a number of effects including acoustic scattering and diffraction and differences in sensor directivity, placement, and size.

B. Laser-ablation sound source

A pulsed laser focused to a small spot on a surface can deposit a vast amount of energy in a short amount of time [58]. This phenomenon has fueled diverse technologies, including micromachining [59], laser-induced-breakdown spectroscopy [60], thin-film growth [61], and a platform for studies of light-plasma interactions [62]. The sharp acoustic impulse generated by laser ablation has spurred its own research thrusts on noncontact damage detection [63], medical imaging [64], and scale-modeling of sonic booms [65]. The impulse has an N-shaped acoustic signature, consisting of a sharp rise followed by a decay through a zero crossing into a slower-time-scale trough.

In our second set of experiments, we use laser ablation to generate high-frequency-content impulsive sounds to test the high-frequency measurement capabilities of our microsphere-based acoustic sensor. The ablation laser

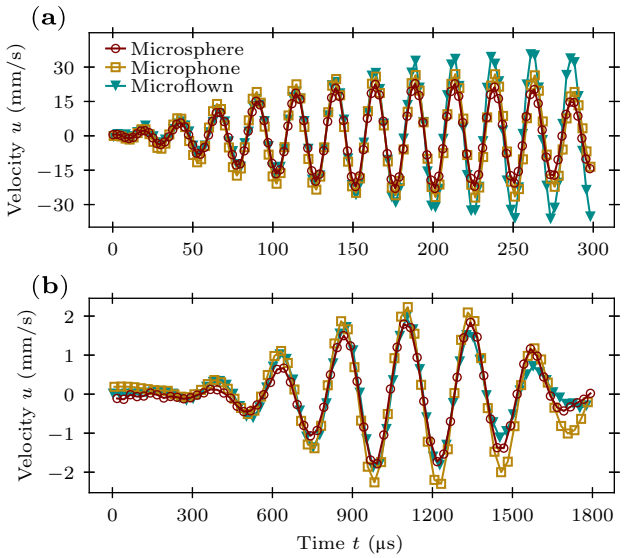

FIG. 5. Comparing measurements of tone-burst signals between three acoustic sensors. (a) Ten cycles of a 40 kHz tone (9 V peak-to-peak drive voltage). All sensors are postprocessed to a bandwidth of 200 kHz. (b) Three cycles of a 4 kHz tone (7 V peak-to-peak drive voltage). All sensors are postprocessed to a bandwidth of 20 kHz. In both panels, 100 independent trials are averaged and the origin in time is aligned for each sensor manually.

operates at a wavelength of 532 nm with a pulse width of 5 ns and an energy of approximately 7 mJ. The pulse has a flat-top mode shape that is focused with a 65 mm focal length lens to approximately 75 μm on an aluminum target. The ablation target, focusing lens, and laser steering mirror are all mounted on the motorized platform used to vary the source distance Δx. The ablation target is further motorized to rotate and reveal a fresh target spot every ten shots. For this experiment, we do not measure the Microflown signal because of its limited high-frequency sensitivity.

Figure 6 shows the microphone and microsphere signals at $\Delta x = 100$ mm. It is well known that standard microphones are unable to resolve the rising edge of the acoustic impulse sourced by laser ablation [66], necessitating alternative methods such as laser deflection or interference [35]. Our results indicate that optically trapped microspheres offer another alternative that is capable of measuring impulsive signals with an approximately 1 μs rising edge, defined as the time for the signal to change from 10% to 90% of its peak value. By comparison, the microphone measures a rise time of approximately 5 μs. As Δx decreases, the microsphere signal becomes more intricate, featuring two or more initial peaks (see Fig. 8 of the Appendix). The details of these features are very sensitive to the orientation of the target and its lateral offset from the trap center.

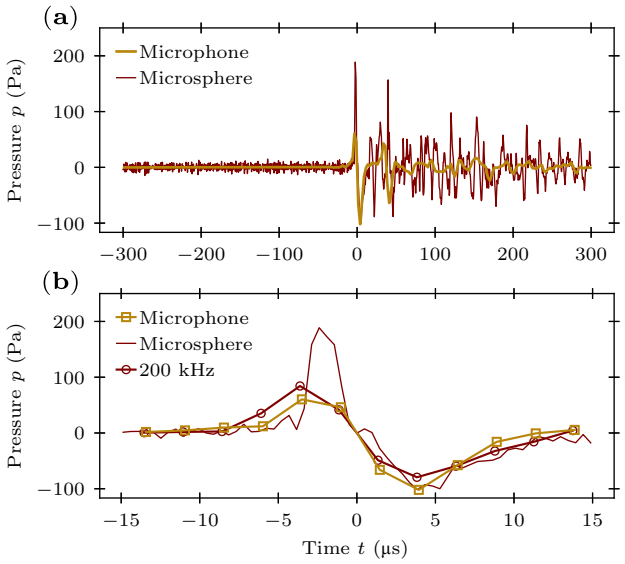

FIG. 6. The microsphere and microphone response to an acoustic impulse generated by laser ablation, averaged over ten shots. (a) A trace showing the initial noise level, the leading-edge arrival, and subsequent reverberations. The microphone is processed with its maximum bandwidth of 200 kHz and the microsphere is processed with a bandwidth of 1 MHz. The time origin is set to the first zero crossing following the leading edge. (b) A trace of the same impulse over a 20× shorter time window. The solid red line is for the microsphere data shown in (a), the open squares are the microphone data, and the open circles are the microsphere data filtered to a bandwidth of 200 kHz.

IV. DISCUSSION

We now turn to a discussion of the results presented in Sec. III. We then contextualize the results by reviewing similar work using optically trapped microspheres for flow measurements. Finally, we outline possible extensions and applications left for future work.

From the tone-burst experiments, we conclude that our microsphere-based acoustic sensor is capable of making calibrated acoustic measurements. All three sensors agree well when converted to the same units, suggesting that the plane-wave impedance model is acceptable and that our microsphere calibration and sensing protocol are correct. The laser-ablation sound source highlights the superior bandwidth of the microsphere in the form of a steeper rising edge and higher peak pressure as compared to the microphone. In the trough portion of the ablation signal, the two sensors are in better quantitative agreement because the acoustic variations are slower and therefore less susceptible to band-limited distortion. When the analysis bandwidth of the microsphere is restricted to that of the microphone [open circles in Fig. 6(b)], the rise times and peak pressures are in much better agreement. Unlike the tone-burst sources, shorter source distances Δx result in worse agreement between the microsphere and microphone for laser-ablation sources. We understand this as a near-field source impedance effect. Indeed, laser-ablation acoustic waves are typically modeled as spherical or cylindrical waves, for which the impedance is a complex-valued function that approaches to the plane-wave value at large source distances Δx. Taken together, our experiments show that optically trapped microspheres enable calibrated and high-bandwidth sensing of the velocity quadrature of an acoustic wave.

Let us next contrast our microsphere-based sensing protocol with other experiments in the recent literature. First, one other work has couched their experiments as acoustic sensing using optically trapped microspheres [29] but in a dramatically different regime. In that work, a 60-nm gold sphere is trapped in water and imaged at 50 Hz with a camera. Sounds are generated by intensity modulating a cw laser beam focused onto a nearby cluster of gold nanoparticles at 10–50 Hz or by a needle attached to a 300 Hz loudspeaker. Since the detection method is slow, the methodology hinges on measuring the position variance of the particle in response to sound; hence no time-dependent waveforms may be constructed. The authors claim to be able to detect sound power down to a level of $-60\ \mathrm{dB}_{\mathrm{re\ 1pW}}$. Similar frequency-domain analysis of camera-captured microsphere trajectories is used in Ref. [27], where flow is generated by the rotating flagella bundle of an optically trapped bacterium, and in Ref. [28], where flow is generated by periodically blocking and unblocking one of two transversely separated traps, causing a drive particle to jump periodically. In Ref. [32], a microsphere is trapped in water contained within a 6.8 MHz piezo-driven standing-wave chamber. The time-averaged microsphere position is recorded using a camera at 150 Hz. The steady-state displacement of the microsphere from its equilibrium position maps the standing-wave profile. In a more recent work termed *optical tweezer-based velocimetry* [30], a position-sensitive detector monitors a microsphere optically trapped in a water-filled sample chamber. The sample chamber is driven at frequencies of 1–90 Hz. Velocity amplitudes of 1.5–70 μm/s are detected in real time. Such low amplitudes beat the thermal limit by using a Kalman filter to deduce the flow velocity from the microsphere position measurements in the presence of Brownian motion. In another recent work [31], a silica microsphere is optically trapped in water and driven transversely at 50–400 Hz. An additional 30 smaller polystyrene tracer particles, initially optically trapped at fixed locations near the drive particle, are released upon starting the drive and observed to follow Lissajous trajectories. Our method makes quantitative acoustic field measurements in air with enough time resolution to observe acoustic waveforms at 4 kHz and 40 kHz, as well as impulsive waveforms with frequency content in the megahertz range. Like some of the above methods, our method measures the flow velocity of the surrounding fluid. However, instead of inferring the flow velocity through the average displacement of

the microsphere, we rely on high-speed position measurements capable of resolving instantaneous velocity and a hydrodynamic model of the viscous coupling between fluid and microsphere, thereby dramatically increasing the detection bandwidth.

Our results set up numerous opportunities for follow-up work. First, incorporating a Kalman filter could increase the signal-to-noise ratio while preserving the ability to self-calibrate. Second, our demonstration has been in air but the theory is equally valid in liquid. Acoustic transduction in a liquid is more efficient than in a gas due to a greater similarity in acoustic impedance between the solid transducer and the medium in which the sound propagates. Therefore, it would be interesting to compare our method to state-of-the-art acoustic sensors for water, such as a needle hydrophone. One could also consider acoustic transduction in microscopic heterogeneous aqueous environments, such as a living cell. However, our thermomechanical calibration scheme requires accurate knowledge of the medium and even simple salt-water solutions can dramatically alter the viscosity of water, so significant uncertainties can be expected in complex media. Finally, since the microsphere measures the acoustic velocity, it could be combined with novel optoacoustic methods that are capable of high-bandwidth pressure measurement to elucidate the impedance of unique sources such as blast waves from laser ablation, surface acoustic waves, and surface vibrations in the near field. Further, since velocity is a vector quantity, the microsphere could be useful in sound-source localization, opening the door to several applications. Applications of high-bandwidth acoustic velocity sensing could include locating where a firearm has been discharged, real-time monitoring in proton-therapy for cancer treatment [67,68], and event discrimination in bubble-chamber searches for dark matter [69–71].

V. CONCLUSIONS

By monitoring the instantaneous velocity of an optically trapped microsphere, we infer the fluid flow of sonic, ultrasonic, and impulsive perturbations in air. We validate the accuracy of our technique by comparing tone-burst measurements made with two commercially available devices, a high-bandwidth pressure microphone and a dual-hot-wire anemometer—the Microflown—that measures acoustic velocity. We then test the bandwidth of our sensor by exposing it to impulsive test sounds generated by laser ablation. Beyond the direct extensions mentioned in Sec. IV, we hope that this work will inspire other sensing protocols enabled by the resolution of the instantaneous velocity of a Brownian particle.

ACKNOWLEDGMENTS

We thank Neal Hall for several useful discussions.

APPENDIX: SOUND-DETECTION RESULTS FOR VARIOUS SOURCE DISTANCES

In this appendix, we display measurement results like those reported in Sec. III, but for various source-to-sensor distances Δx. Figure 7 considers the tone-burst

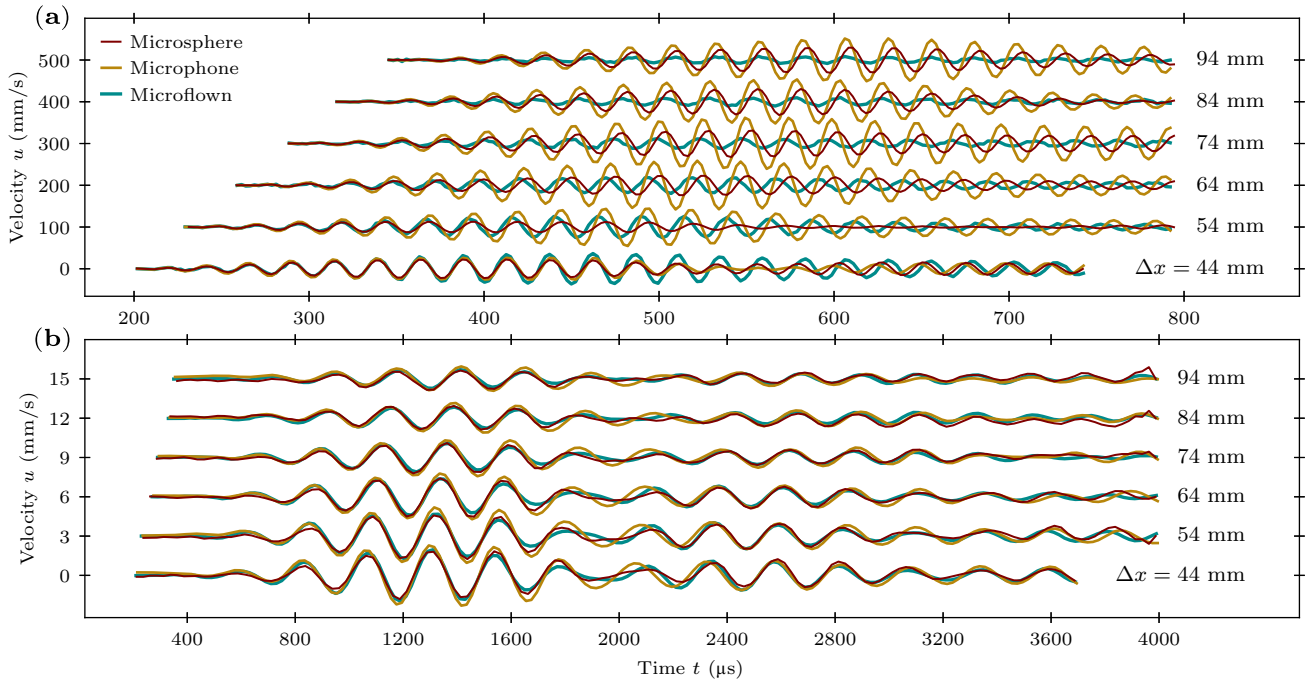

FIG. 7. The tone-burst detection results as in Fig. 5 but for various source distances Δx and for a (a) 40 kHz and (b) 4 kHz drive. The traces corresponding to different source distances are vertically shifted for clarity.

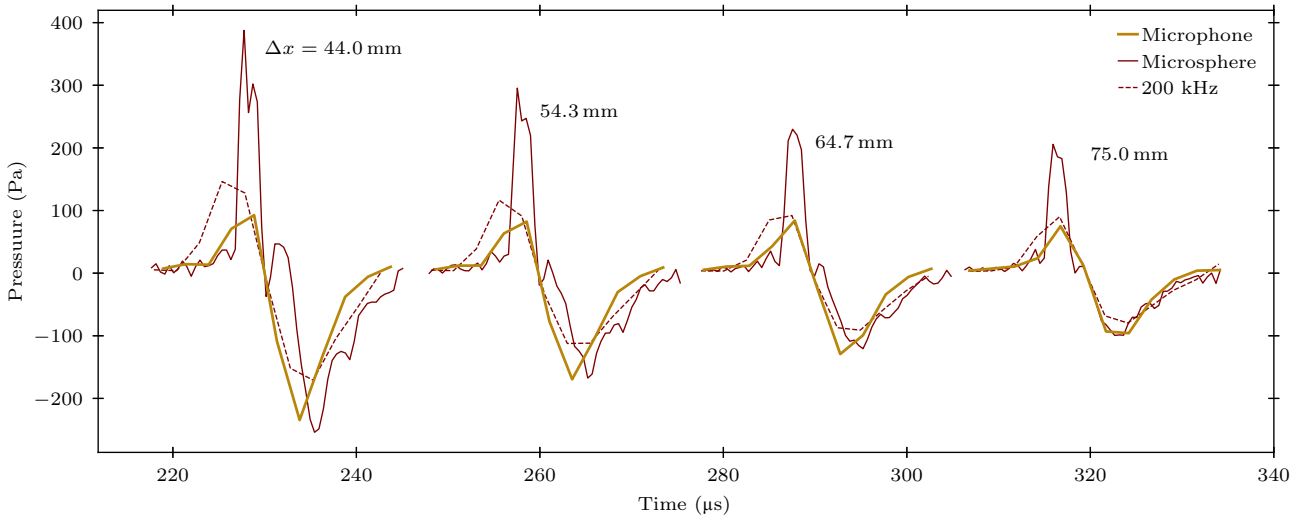

FIG. 8. The laser-ablation detection results as in Fig. 6 but for various source distances Δx.

sound source and Fig. 8 considers the laser-ablation sound source.

[1] G. Volpe, O. M. Maragò, H. Rubinsztein-Dunlop, G. Pesce, A. B. Stilgoe, G. Volpe, G. Tkachenko, V. G. Truong, S. N. Chormaic, and F. Kalantarifard, *et al.*, Roadmap for optical tweezers, J. Phys.: Photonics **5**, 022501 (2023).

[2] A. Ashkin, Acceleration and trapping of particles by radiation pressure, Phys. Rev. Lett. **24**, 156 (1970).

[3] A. Ashkin and J. M. Dziedzic, Optical levitation in high vacuum, Appl. Phys. Lett. **28**, 333 (1976).

[4] G. Ranjit, M. Cunningham, K. Casey, and A. A. Geraci, Zeptonewton force sensing with nanospheres in an optical lattice, Phys. Rev. A **93**, 053801 (2016).

[5] J. Ahn, Z. Xu, J. Bang, P. Ju, X. Gao, and T. Li, Ultrasensitive torque detection with an optically levitated nanorotor, Nat. Nanotechnol. **15**, 89 (2020).

[6] D. C. Moore and A. A. Geraci, Searching for new physics using optically levitated sensors, Quantum Sci. Technol. **6**, 014008 (2021).

[7] A. Arvanitaki and A. A. Geraci, Detecting high-frequency gravitational waves with optically levitated sensors, Phys. Rev. Lett. **110**, 071105 (2013).

[8] T. Li, S. Kheifets, and M. G. Raizen, Millikelvin cooling of an optically trapped microsphere in vacuum, Nat. Phys. **7**, 527 (2011).

[9] U. Delić, M. Reisenbauer, K. Dare, D. Grass, V. Vuletić, N. Kiesel, and M. Aspelmeyer, Cooling of a levitated nanoparticle to the motional quantum ground state, Science **367**, 892 (2020).

[10] J. Piotrowski, D. Windey, J. Vijayan, C. Gonzalez-Ballestero, A. de los Ríos Sommer, N. Meyer, R. Quidant, O. Romero-Isart, R. Reimann, and L. Novotny, Simultaneous ground-state cooling of two mechanical modes of a levitated nanoparticle, Nat. Phys. **19**, 1009 (2023).

[11] S. Ebadi, T. T. Wang, H. Levine, A. Keesling, G. Semeghini, A. Omran, D. Bluvstein, R. Samajdar, H. Pichler, W. W. Ho, S. Choi, S. Sachdev, M. Greiner, V. Vuletić, and M. D. Lukin, Quantum phases of matter on a 256-atom programmable quantum simulator, Nature **595**, 227 (2021).

[12] D. Bluvstein, H. Levine, G. Semeghini, T. T. Wang, S. Ebadi, M. Kalinowski, A. Keesling, N. Maskara, H. Pichler, M. Greiner, V. Vuletić, and M. D. Lukin, A quantum processor based on coherent transport of entangled atom arrays, Nature **604**, 451 (2022).

[13] A. Ashkin and J. M. Dziedzic, Optical trapping and manipulation of viruses and bacteria, Science **235**, 1517 (1987).

[14] A. Ashkin, J. M. Dziedzic, and T. Yamane, Optical trapping and manipulation of single cells using infrared laser beams, Nature **330**, 769 (1987).

[15] A. Gennerich, ed., *Optical Tweezers Methods and Protocols*, Methods in Molecular Biology (Springer Science + Business Media, New York, 2017).

[16] K. Svoboda and S. M. Block, Biological applications of optical forces, Annu. Rev. Biophys. Biomol. Struct. **23**, 247 (1994).

[17] K. Svoboda, C. F. Schmidt, B. J. Schnapp, and S. M. Block, Direct observation of kinesin stepping by optical trapping interferometry, Nature **365**, 721 (1993).

[18] L. S. Madsen, M. Waleed, C. A. Casacio, A. Terrasson, A. B. Stilgoe, M. A. Taylor, and W. P. Bowen, Ultrafast viscosity measurement with ballistic optical tweezers, Nat. Photonics **15**, 386 (2021).

[19] L. B. Pires, D. S. Ether, B. Spreng, G. R. S. Araújo, R. S. Decca, R. S. Dutra, M. Borges, F. S. S. Rosa, G.-L. Ingold, M. J. B. Moura, S. Frases, B. Pontes, H. M. Nussenzveig, S. Reynaud, N. B. Viana, and P. A. Maia Neto, Probing the screening of the Casimir interaction with optical tweezers, Phys. Rev. Res. **3**, 033037 (2021).

[20] A. Kalume, C. Wang, and Y.-L. Pan, Optical-trapping laser techniques for characterizing airborne aerosol particles and its application in chemical aerosol study, Micromachines **12**, 466 (2021).

[21] C. P. Blakemore, D. Martin, A. Fieguth, A. Kawasaki, N. Priel, A. D. Rider, and G. Gratta, Absolute pressure and gas species identification with an optically levitated rotor,

J. Vac. Sci. Technol. B, Nanotechnol. Microelectronics: Mater. Process. Meas. Phenom. **38**, 024201 (2020).

[22] L. E. Hillberry, Y. Xu, S. Miki-Silva, G. H. Alvarez, J. E. Orenstein, L. C. Ha, D. S. Ether, and M. G. Raizen, Weighing an optically trapped microsphere in thermal equilibrium with air, Phys. Rev. Appl. **14**, 044027 (2020).

[23] G. Carlse, K. B. Borsos, H. C. Beica, T. Vacheresse, A. Pouliot, J. Perez-Garcia, A. Vorozcovs, B. Barron, S. Jackson, L. Marmet, and A. Kumarakrishnan, Technique for rapid mass determination of airborne microparticles based on release and recapture from an optical dipole force trap, Phys. Rev. Appl. **14**, 024017 (2020).

[24] A. Ashkin and J. M. Dziedzic, Optical levitation of liquid drops by radiation pressure, Science **187**, 1073 (1975).

[25] N. Magome, M. I. Kohira, E. Hayata, S. Mukai, and K. Yoshikawa, Optical trapping of a growing water droplet in air, J. Phys. Chem. B **107**, 3988 (2003).

[26] S. ishizaka, T. Wada, and N. Kitamura, In situ observations of freezing processes of single micrometer-sized aqueous ammonium sulfate droplets in air, Chem. Phys. Lett. **506**, 117 (2011).

[27] S. R. Kirchner, S. Nedev, S. Carretero-Palacios, A. Mader, M. Opitz, T. Lohmüller, and J. Feldmann, Direct optical monitoring of flow generated by bacterial flagellar rotation, Appl. Phys. Lett. **104**, 093701 (2014).

[28] S. Nedev, S. Carretero-Palacios, S. R. Kirchner, F. Jäckel, and J. Feldmann, Microscale mapping of oscillatory flows, Appl. Phys. Lett. **105**, 161113 (2014).

[29] A. Ohlinger, A. Deak, A. A. Lutich, and J. Feldmann, Optically trapped gold nanoparticle enables listening at the microscale, Phys. Rev. Lett. **108**, 018101 (2012).

[30] P. G. Dehnavi, D. Wei, M.-E. Aubin-Tam, and D. S. W. Tam, Optical tweezers-based velocimetry: A method to measure microscale unsteady flows, Exp. Fluids **61**, 1 (2020).

[31] N. Bruot, P. Cicuta, H. Bloomfield-Gadêlha, R. E. Goldstein, J. Kotar, E. Lauga, and F. Nadal, Direct measurement of unsteady microscale Stokes flow using optically driven microspheres, Phys. Rev. Fluids **6**, 053102 (2021).

[32] P. G. Bassindale, D. B. Phillips, A. C. Barnes, and B. W. Drinkwater, Measurements of the force fields within an acoustic standing wave using holographic optical tweezers, Appl. Phys. Lett. **104**, 163504 (2014).

[33] S. Basiri-Esfahani, A. Armin, S. Forstner, and W. P. Bowen, Precision ultrasound sensing on a chip, Nat. Commun. **10**, 132 (2019).

[34] S.-J. Tang, M. Zhang, J. Sun, J.-W. Meng, X. Xiong, Q. Gong, D. Jin, Q.-F. Yang, and Y.-F. Xiao, Single-particle photoacoustic vibrational spectroscopy using optical microresonators, Nat. Photonics **17**, 951 (2023).

[35] G. Wissmeyer, M. A. Pleitez, A. Rosenthal, and V. Ntziachristos, Looking at sound: Optoacoustics with all-optical ultrasound detection, Light: Sci. Appl. **7**, 53 (2018).

[36] T. Li, S. Kheifets, D. Medellin, and M. G. Raizen, Measurement of the instantaneous velocity of a Brownian particle, Science **328**, 1673 (2010).

[37] S. Kheifets, A. Simha, K. Melin, T. Li, and M. G. Raizen, Observation of Brownian motion in liquids at short times: Instantaneous velocity and memory loss, Science **343**, 1493 (2014).

[38] Z. Chen, T. Kuang, X. Han, G. Li, W. Zeng, W. Xiong, G. Xiao, and H. Luo, Differential displacement measurement of the levitated particle using D-shaped mirrors in the optical tweezers, Opt. Express **30**, 30791 (2022).

[39] H.-E. de Bree, W. F. Druyvesteyn, E. Berenschot, and M. Elwenspoek, in *Technical Digest. IEEE International MEMS 99 Conference. Twelfth IEEE International Conference on Micro Electro Mechanical Systems (Cat. No. 99CH36291)* (IEEE, 1999), p. 124.

[40] H.-E. de Bree, An overview of microflown technologies, Acta Acust. United Acust. **89**, 163 (2003).

[41] H.-E. de Bree, The Microflown e-book, https://www.microflown.com/resources/e-books/e-book-the-microflown-e-book (2009), accessed: 18 October 2022.

[42] R. Brown, A brief account of microscopical observations made in the months of June, July and August 1827, on the particles contained in the pollen of plants; and on the general existence of active molecules in organic and inorganic bodies, Philos. Mag. **4**, 161 (1828).

[43] S. Kheifets, Ph.D. thesis, The University of Texas at Austin, 2014.

[44] J. Mo, A. Simha, and M. G. Raizen, Broadband boundary effects on Brownian motion, Phys. Rev. E **92**, 062106 (2015).

[45] A. Premlata and H.-H. Wei, Atypical non-Basset particle dynamics due to hydrodynamic slip, Phys. Fluids **32**, 097109 (2020).

[46] A. B. Basset, On the motion of a sphere in a viscous liquid, Philos. Trans. R. Soc. London, A **179**, 43 (1888).

[47] M. R. Maxey and J. J. Riley, Equation of motion for a small rigid sphere in a nonuniform flow, Phys. Fluids **26**, 883 (1983).

[48] S. Temkin and C.-M. Leung, On the velocity of a rigid sphere in a sound wave, J. Sound Vib. **49**, 75 (1976).

[49] G. G. Stokes, On the effect of the internal friction of fluids on the motion of pendulums, Trans. Cambridge Philos. Soc. **9**, 8 (1851).

[50] L. D. Landau and E. M. Lifshitz, *Fluid Mechanics: Course of Theoretical Physics, Volume 6* (Pergamon Press, New York, 2013), Vol. 6.

[51] P. T. Tsilingiris, Review and critical comparative evaluation of moist air thermophysical properties at the temperature range between 0 and 100°C for engineering calculations, Renew. Sust. Energ. Rev. **83**, 50 (2018).

[52] S. F. Norrelykke and H. Flyvbjerg, Power spectrum analysis with least-squares fitting: Amplitude bias and its elimination, with application to optical tweezers and atomic force microscope cantilevers, Rev. Sci. Instrum. **81**, 075103 (2010).

[53] J. Tóthová and V. Lisỳ, A note on the fluctuation-dissipation relation for the generalized Langevin equation with hydrodynamic backflow, Phys. Lett. A **380**, 2561 (2016).

[54] R. Kubo, The fluctuation-dissipation theorem, Rep. Prog. Phys. **29**, 255 (1966).

[55] W. Stöber, A. Fink, and E. Bohn, Controlled growth of monodisperse silica spheres in the micron size range, J. Colloid Interface Sci. **26**, 62 (1968).

[56] C. Dawson and J. Bateman, Spectral analysis and parameter estimation in levitated optomechanics, J. Opt. Soc. Am. B **36**, 1565 (2019).

[57] Sunaina, M. Butola, and K. Khare, Calculating numerical derivatives using Fourier transform: Some pitfalls and how to avoid them, Eur. J. Phys. **39**, 065806 (2018).

[58] T. W. Murray and J. W. Wagner, Laser generation of acoustic waves in the ablative regime, J. Appl. Phys. **85**, 2031 (1999).

[59] X. Liu, D. Du, and G. Mourou, Laser ablation and micromachining with ultrashort laser pulses, IEEE. J. Quantum Electron. **33**, 1706 (1997).

[60] C. Pasquini, J. Cortez, L. Silva, and F. B. Gonzaga, Laser induced breakdown spectroscopy, J. Braz. Chem. Soc. **18**, 463 (2007).

[61] D. Dijkkamp, T. Venkatesan, X. Wu, S. Shaheen, N. Jisrawi, Y. Min-Lee, W. McLean, and M. Croft, Preparation of Y-Ba-Cu oxide superconductor thin films using pulsed laser evaporation from high T_c bulk material, Appl. Phys. Lett. **51**, 619 (1987).

[62] P. Gibbon and E. Förster, Short-pulse laser-plasma interactions, Plasma Phys. Control. Fusion **38**, 769 (1996).

[63] I. Kajiwara, R. Akita, and N. Hosoya, Damage detection in pipes based on acoustic excitations using laser-induced plasma, Mech. Syst. Signal Process. **111**, 570 (2018).

[64] L. V. Wang and S. Hu, Photoacoustic tomography: In vivo imaging from organelles to organs, Science **335**, 1458 (2012).

[65] Q. Qin and K. Attenborough, Characteristics and application of laser-generated acoustic shock waves in air, Appl. Acoust. **65**, 325 (2004).

[66] J.-L. Thomas, R. Marchiano, and D. Baresch, Acoustical and optical radiation pressure and the development of single beam acoustical tweezers, J. Quant. Spectrosc. Radiat. Transfer **195**, 55 (2017).

[67] M. De Matteis, A. Baschirotto, and E. Vallicelli, Acoustic analog signal processing for 20–200 MeV proton sound detectors, IEEE Trans. Radiat. Plasma Med. Sci. **6**, 325 (2021).

[68] F. R. Deurvorst, G. Collado Lara, A. Matalliotakis, H. J. Vos, N. De Jong, V. Daeichin, and M. D. Verweij, A spatial and temporal characterisation of single proton acoustic waves in proton beam cancer therapy, J. Acoust. Soc. Am. **151**, 1200 (2022).

[69] E. Behnke, J. Behnke, S. J. Brice, D. Broemmelsiek, J. I. Collar, P. S. Cooper, M. Crisler, C. E. Dahl, D. Fustin, and J. Hall, *et al.*, Improved limits on spin-dependent WIMP-proton interactions from a two liter CF_3I bubble chamber, Phys. Rev. Lett. **106**, 021303 (2011).

[70] T. Kozynets, S. Fallows, and C. B. Krauss, Modeling emission of acoustic energy during bubble expansion in pico bubble chambers, Phys. Rev. D. **100**, 052001 (2019).

[71] C. Amole, *et al.*, PICO Collaboration, Dark matter search results from the complete exposure of the PICO-60 C_3F_8 bubble chamber, Phys. Rev. D. **100**, 022001 (2019).